

LA-UR-18-21681 (Accepted Manuscript)

Physics design of the next-generation spallation neutron target-moderator-reflector-shield assembly at LANSCE

Zavorka, Lukas
Mocko, Michael Jeffrey
Koehler, Paul E.

Provided by the author(s) and the Los Alamos National Laboratory (2018-09-26).

To be published in: Nuclear Instruments and Methods in Physics Research Section A: Accelerators, Spectrometers, Detectors and Associated Equipment

DOI to publisher's version: 10.1016/j.nima.2018.06.018

Permalink to record: <http://permalink.lanl.gov/object/view?what=info:lanl-repo/lareport/LA-UR-18-21681>

Disclaimer:

Approved for public release. Los Alamos National Laboratory, an affirmative action/equal opportunity employer, is operated by the Los Alamos National Security, LLC for the National Nuclear Security Administration of the U.S. Department of Energy under contract DE-AC52-06NA25396. Los Alamos National Laboratory strongly supports academic freedom and a researcher's right to publish; as an institution, however, the Laboratory does not endorse the viewpoint of a publication or guarantee its technical correctness.

Physics design of the next-generation spallation neutron target-moderator-reflector-shield assembly at LANSCE

Lukas Zavorka*, Michael J. Mocko, and Paul E. Koehler

Los Alamos National Laboratory, P.O. Box 1663, Los Alamos, NM 87545, United States

Abstract

We discuss the physics design of the next-generation spallation neutron target-moderator-reflector-shield (TMRS) assembly for the Manuel Lujan Jr. Neutron Scattering Center (Lujan Center) at the Los Alamos Neutron Science Center (LANSCE). We developed this TMRS to improve the neutronic performance of the Lujan Center in the intermediate energy range (keV-MeV) enabling a variety of new nuclear physics experiments, as well as increasing the quality of the ongoing experiments. The results of our Monte Carlo optimization study indicate that the new TMRS will generate keV-MeV neutrons with higher intensity and improved time resolution. At the same time, the new design largely maintains its current performance in the cold and thermal ranges supporting materials research. In this article we show that the new TMRS has the potential to enhance the Lujan Center's experimental capability in a wider interval of energies—cold to intermediate—after its scheduled installation in 2020.

Keywords: Spallation neutron generation, Neutron time-of-flight facility, MCNPX optimization study

1. Introduction

1 The currently operating TMRS assembly, known as Mark-III [1], has been providing neu-
2 trons to the scientific instruments of the Lujan Center at LANSCE [2] since 2010. Neutrons
3 are generated in the spallation process initiated by the 800-MeV protons supplied by the linear
4 accelerator. The proton beam impinges a split tungsten target after its compression from 625- μ s
5 to 125-ns pulses (FWHM) in a proton storage ring with a typical current $\sim 100 \mu\text{A}$ at a repetition
6 rate of 20 Hz. The produced neutrons are slowed down and moderated in a moderator-reflector
7 assembly surrounding the target and the resulting cold and thermal neutron beams are delivered
8 to the instruments via neutron flight paths (FPs).

9 The lifetime of the Lujan TMRS is primarily limited by radiation damage to the proton beam
10 window and the tungsten target. Based on our operating experience, the lifetime translates to
11 about 2500 mA*h of protons delivered. Our schedule indicates that we will have reached this
12 limit by 2020. The forthcoming replacement is an opportunity to implement the design modifi-
13 cations that will improve the neutronic performance of the new TMRS in the keV-MeV energy
14

*Corresponding author

Email address: zavorka@lanl.gov (Lukas Zavorka)

15 range. At the same time, the new TMRS shall maintain its existing capability to support materials
16 research with cold and thermal neutrons.

17 The keV-MeV range is key for a large number of basic and applied nuclear science efforts,
18 particularly related to neutron capture and resonance total cross section measurements. The
19 fission neutron spectrum in fast reactors contains a substantial flux in the keV-MeV region, which
20 has historically been challenging to measure accurately [3]. Further, measurements in the 1-
21 500 keV range are essential for a large number of astrophysical applications, where the increased
22 neutron intensity opens the door to a wider range of measurements on unstable targets [4]. In
23 addition to expanding existing measurements, the superior generation of keV-MeV neutrons will
24 enable a new capability for total cross section measurements [5, 6]. Lastly, improved neutronic
25 performance in the keV-MeV range will enable the stockpile stewardship program to conduct
26 the (n,γ) measurements with radioactive samples of a reduced size. The improved signal-to-
27 background ratio of such measurements will reduce experimental uncertainties, which currently
28 reach 20% to 50% at 1 MeV in the case of $^{239}\text{Pu}(n,\gamma)$ [7].

29 Mark-III moderators and FPs are arranged in two vertical tiers. For the new TMRS, we
30 propose an arrangement in which one tier (the upper tier) has been radically redesigned and
31 optimized for nuclear science in the keV-MeV energies, and the other tier (the lower tier) has
32 largely been left unmodified to keep providing cold and thermal neutrons for materials research.
33 These two tiers are neutronicly separated as much as possible.

34 The article starts with a description of the existing Mark-III TMRS assembly. In Section 2
35 we explain why is not this assembly optimal for nuclear science in the keV-MeV interval. We
36 conclude the section by presenting the MCNPX model of the TMRS and its validation against
37 experimental data. Subsequently in Section 3, we introduce the physics design of the next-
38 generation TMRS Mark-IV, which was built upon the validated Mark-III geometry. We discuss
39 major upper-tier modifications that significantly increase the figure of merit, which incorporates
40 performance characteristics in both neutron flux and time resolution. The section includes a
41 description of the redesigned high-resolution water moderator supporting materials research in
42 the lower tier. Finally, in Section 4 we show that the new Lujan target would benefit from a more
43 flexible regime of operation.

44 2. Current Mark-III TMRS design

45 The Mark-III TMRS is a research facility that generates cold and thermal neutrons for a vari-
46 ety of scientific disciplines, such as fundamental and applied nuclear physics, materials research,
47 chemistry, and biology. Mark-III originated from the first-generation TMRS, known as Mark-0,
48 which started to operate at the Lujan Center in 1985 [8]. Since then, a significant number of de-
49 sign modifications have been implemented in the three subsequent TMRS generations, including
50 decoupled, partially coupled, and backscattering moderators [9, 10]; composite beryllium-lead
51 and stainless steel reflectors [11]; and, most recently, a cold beryllium reflector-filter [1].

52 The current Lujan TMRS (see Figure 1) is cylindrical, 60 cm in diameter and approximately
53 3 m in height. It is inserted into a steel vacuum vessel which contains a lead reflector-shield
54 and the beam stop. The vessel is surrounded by approximately 3 m of biological shielding
55 made of steel and heavy concrete. The incident proton beam has a 2D Gaussian spatial profile
56 with FWHM ≈ 3.5 cm. It enters the TMRS vertically through a water-cooled beam window
57 manufactured from Inconel-718. The beam impinges the split cylindrical tungsten target with a
58 diameter of 10 cm. The target is surrounded by a bulk beryllium reflector to improve neutron
59 economy.

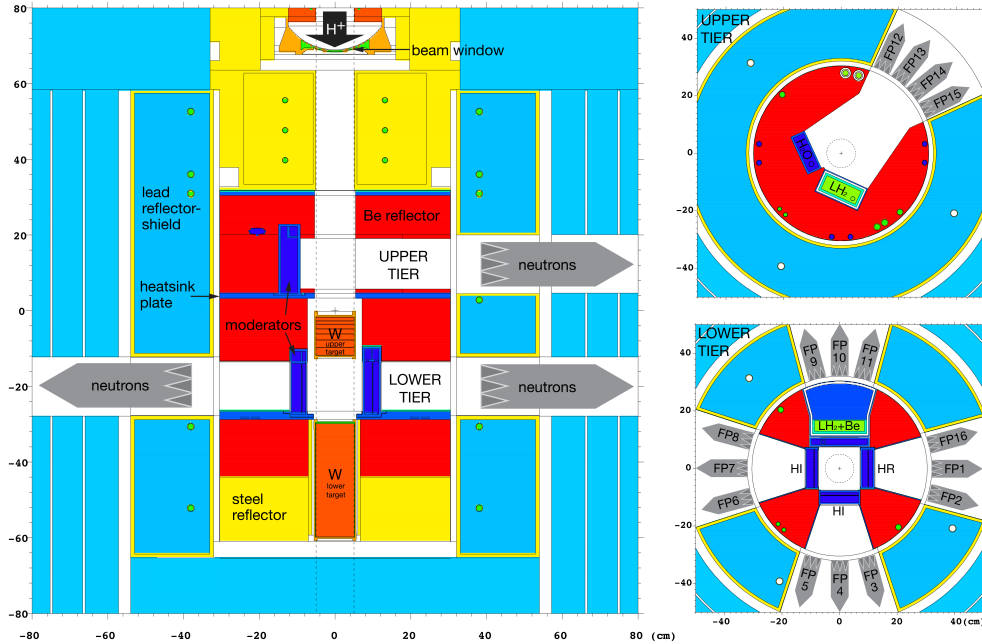


Figure 1: Elevation (left) and plane (right) views through the Mark-III geometry showing an arrangement of upper-tier backscattering moderators (top right) and lower-tier high-intensity (HI) and high-resolution (HR) moderators and a cold beryllium reflector-filter (bottom right).

60 There are six neutron moderators arranged in two vertical tiers. The upper tier is composed
 61 of two coupled backscattering moderators, one of which is filled with chilled water and the
 62 other with liquid hydrogen. Each moderator serves two FPs. The lower tier encompasses four
 63 moderators in the flux-trap geometry [12]: three pre-moderated decoupled water moderators and
 64 one pre-moderated partially coupled liquid hydrogen moderator with a cold beryllium reflector-
 65 filter. Two of the decoupled water moderators are designated as high-intensity (HI) and one as
 66 high-resolution (HR). The resolution of the HR moderator refers to the time resolution, which in
 67 fact reflects the energy resolution. The HI and HR moderators differ in gadolinium poison depth.
 68 Each lower-tier moderator can serve up to three FPs. The upper and lower tiers are separated by
 69 a 1.3-cm-thick aluminum heatsink plate.

70 2.1. Performance in the keV-MeV region

71 The Mark-III TMRS was optimized for superior performance in the cold and thermal energy
 72 ranges, while neutrons in the intermediate-energy range and beyond were considered undesirable
 73 background. The Mark-III's bulk beryllium reflector and the lead reflector-shield surrounding
 74 the target increase the chance of neutrons entering a moderator and eventually an FP, but the
 75 reflectors have a predominantly negative impact on time resolution, as neutrons spend more
 76 time in the assembly. The resulting neutron time-emission pulse profiles are rather broad and
 77 asymmetric, with a substantial tail extending to very late times. While the tails can be reduced to
 78 some extent at energies near thermal and below by adding a layer of neutron poison such as Cd

79 or Gd around the moderator and decoupling it from the surrounding components, the long tails
 80 persist for energies above about 1 eV. In addition, the relative width of the time profiles grows
 81 with energy as the mean free path for neutrons increases.

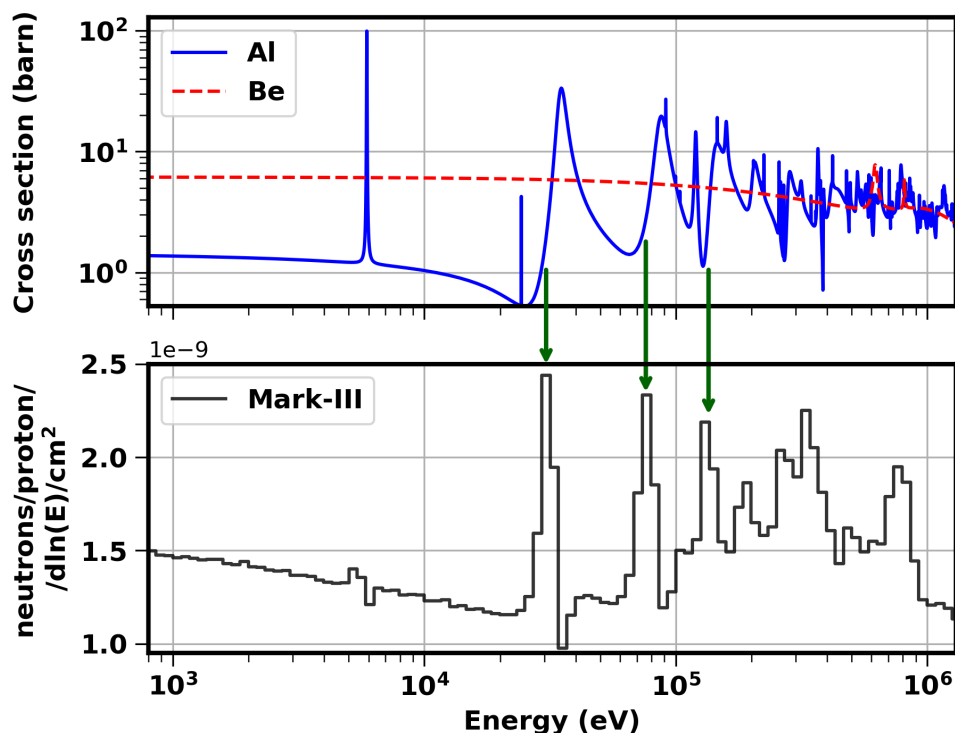


Figure 2: Cross section of neutron elastic scattering in ^9Be and ^{27}Al in the keV-MeV region (top). Neutron flux in the upper-tier FP14 of Mark-III, showing an increase just below the resonances in ^{27}Al (bottom).

82 There is another effect that contributes to the deterioration of the time-emission pulses at
 83 some particular energies. Both ^9Be , which forms the vast majority of the beryllium reflector
 84 except for impurities, and ^{27}Al , which is the main structural material of all Mark-III moderators,
 85 have large cross sections for elastic scattering that exceed 99.95% of the total neutron cross sec-
 86 tion in the keV-MeV region. This phenomenon, combined with rather broad resonances in alu-
 87 minum, starting at approximately 30 keV, contributes to broadening time resolution. As shown
 88 in Figure 2, the neutron flux in the upper-tier FPs increases just below the aluminum resonances
 89 at 35 keV, 88 keV, and 150 keV. But the flux increases at the expense of a dramatic degradation
 90 of time resolution. Figure 3 compares time resolution at 10 keV, where no resonance is present,
 91 with time resolution at 30 keV, i.e., just below the 35-keV resonance, where the FWHM of the
 92 time emission spectrum more than doubles. This degradation is caused by an additional source
 93 of 30-keV neutrons, which arrive with a time delay following the scattering from the 35-keV
 94 resonance into beryllium reflector and back.

95 The broad asymmetric time-emission pulses at intermediate energies present a challenge to
 96 further progress in nuclear science at the Lujan Center. Therefore, both FWHM and the tails of

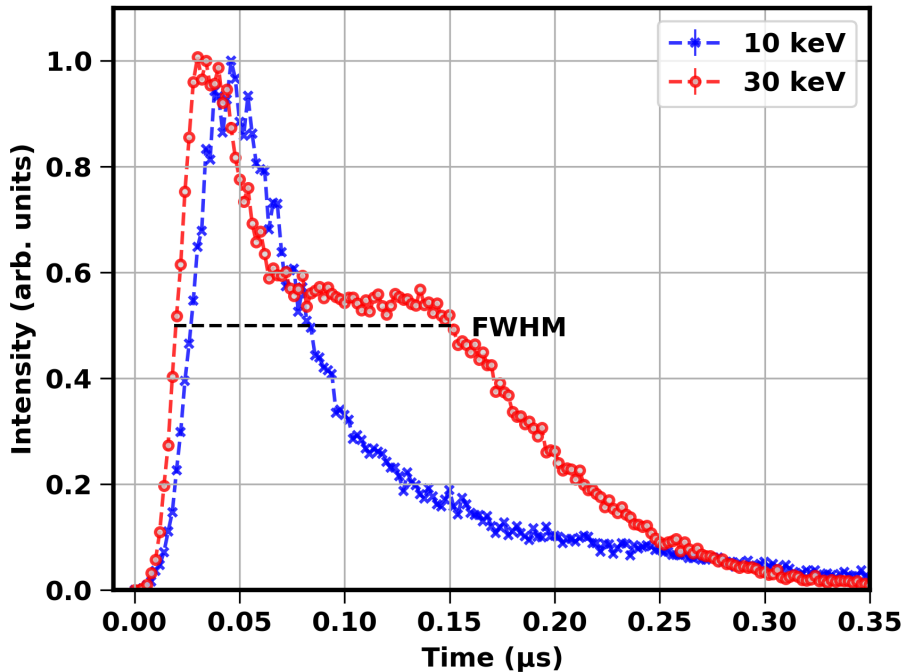


Figure 3: MCNPX simulation of the neutron time-emission spectra in the upper tier of Mark-III. The FWHM at 30 keV more than doubles in comparison with FWHM at 10 keV. The extraordinarily wide pulse at 30 keV is caused by an additional neutron scattering from the 35-keV resonance in ^{27}Al .

107 the time-emission spectra must be reduced, which requires redesigning the TMRS. We anticipate
 108 that the removal of the beryllium reflector and backscattering moderators from the upper tier will
 109 improve time resolution. We also expect that the translation of the existing tungsten target into
 110 the upper tier will increase neutron flux in all of the upper-tier FPs. In this way, the upper tier
 111 shall fit the needs of nuclear science in the keV-MeV interval far better.

102 2.2. Benchmarking of MCNPX models

103 Since the very beginning of the spallation era at LANSCE, the Lujan Center's target physics
 104 team has been developing the detailed MCNPX model of the TMRS assembly. With this model
 105 we perform neutronic optimization studies of the next generations of the Lujan TMRS. We also
 106 use the model for assessing the neutron backgrounds in the neutron scattering experiments and
 107 for carrying out radiation shielding calculations.

108 To ensure the MCNPX model describes the real TMRS's neutronic performance accurately,
 109 a series of experimental measurements of neutron energy spectra and time-emission spectra were
 110 conducted. A general agreement between simulation and measurement, within about 20%, indi-
 111 cates that the team has developed a high-fidelity model [13, 14, 15]. In this work, we build
 112 upon the above-mentioned, and thoroughly benchmarked, model to carry out the Monte Carlo
 113 optimization study of the next-generation TMRS Mark-IV.

114 3. Mark-IV physics design

115 A number of constraints on budget, space, time, engineering requirements, and operational
116 aspects limited the space for developing the new TMRS. The key constraint is that the upper-tier
117 modifications should preserve at least 75% of the thermal neutron flux currently available in the
118 lower tier. Despite all of these constraints, we have designed the next-generation TMRS with a
119 well-optimized performance for both nuclear science and materials research.

120 In the next sections, we present the physics quantities that we studied; then we describe the
121 realities of the redesigned upper tier, followed by a discussion of the proposed modifications to
122 a lower-tier moderator.

123 3.1. Studied physics quantities

124 The neutron flux was calculated using the next-event estimator–point detector of the MCNPX
125 2.7.0 [16]. We used the default physics models, cross sections from ENDF/B [17, 18], and the
126 thermal neutron scattering data $S(\alpha, \beta)$ from ENDF/B-VI [19]. In the upper tier, calculations
127 were carried out for FP14, which serves the DANCE instrument [20], with an actual-size circular
128 field of view (FOV) of $\sim 68 \text{ cm}^2$. In the lower tier, FP2 and FP4 serving the SMARTS [21] and
129 HIPPO [22] instruments, respectively, were selected. These two FPs view the high-resolution
130 and high-intensity moderator, respectively, with the maximum FOV of $12 \times 12 \text{ cm}^2$.

131 The calculated neutron energy spectra are presented as neutron lethargy flux (*neutrons/proton/dln(E)/cm²*).
132 The time-emission spectra are shown as they appear at the boundary of the TMRS. The FWHM
133 of the time-emission spectra is a measure of resolution. It can be expressed as the effective flight-
134 path-length uncertainty L_m . This quantity represents the effective moderator thickness along the
135 beamline and is defined by the non-relativistic formula $L_m = \Delta t_m \cdot \sqrt{E}/72.3$, where the time
136 resolution (FWHM) due to moderator Δt_m is in μs and neutron energy E in eV to obtain L_m in
137 meters [23].

138 It is a common practice to define a single quantity that describes the overall performance of a
139 pulsed neutron source [24]. Here we use a metric called figure of merit (FOM), which combines
140 two very important quantities: neutron flux ϕ and time resolution Δt_m . In the upper tier, we define
141 FOM according to the following equation:

$$FOM(E) = \phi(E)/(\Delta t_m(E))^2. \quad (1)$$

142 Neutron flux (intensity) sets the counting rate and hence determines, for example, the sample
143 size and run duration, whereas time resolution contributes to the ability to resolve peaks caused
144 by neutron interactions with the sample. Discerning these peak properties is vital to most exper-
145 iments.

146 3.2. Upper tier

147 The main modifications that distinguish the upper tier of Mark-IV from the upper tier of
148 Mark-III are the removal of the beryllium reflector and backscattering moderators and the instal-
149 lation of the additional neutron-production target. As shown in Figure 4, the proposed target is
150 a disk perpendicular to the existing split target. The disk target is made of high-density tung-
151 sten, is 10.1 cm in diameter, and is 1.2 cm thick. The target is clad with a 254- μm tantalum
152 layer to prevent water erosion. Water serves as both target coolant and neutron moderator and
153 surrounds the target in a 4-cm-thick rectangular container with 0.2-cm walls made of aluminum

154 and Inconel-718. The new target has a large neutron-emission surface and is relatively thin in the
 155 direction of the FPs, which results in high neutron flux and good time resolution.

156 The water moderator does not aim to fully thermalize neutrons as most conventional moder-
 157 ators do (i.e., to reach the $1/E$ proportionality). Its thickness was optimized for maximal
 158 production of keV-MeV neutrons, and thus it leaves the spectrum undermoderated. A thicker
 159 moderator would promote more thermalization, whereas a thinner moderator would not soften
 160 the spallation neutron spectrum sufficiently.

161 3.2.1. Field of view (FOV)

162 In Mark-III, the upper-tier FPs were designed with the FOV focused on two backscattering
 163 moderators (see Figure 4, where FOV is displayed for FP14). Because these moderators are no
 164 longer present in Mark-IV, it is desired to realign the FPs to focus directly on the center of the
 165 new disk target. In the next sections we call the current Mark-III FP arrangement “FOV Real”
 166 and the desired FP arrangement for Mark-IV “FOV Center.”

167 It is intuitively clear that the neutronic performance of the compact target-moderator sys-
 168 tem depends strongly on an assumed FOV. The emitted neutrons are more uniformly distributed
 169 across the FOV Center, which also provides higher neutron flux and better time resolution. Un-
 170 fortunately, the FP realignment is not in the budget of the TMRS replacement project, but it is
 171 planned to follow the installation of Mark-IV. For this reason, the upper tier has been designed to
 172 accommodate both FOVs. In this paper we present the neutronic performance for both of these
 173 options (i.e., FOV Center and FOV Real).

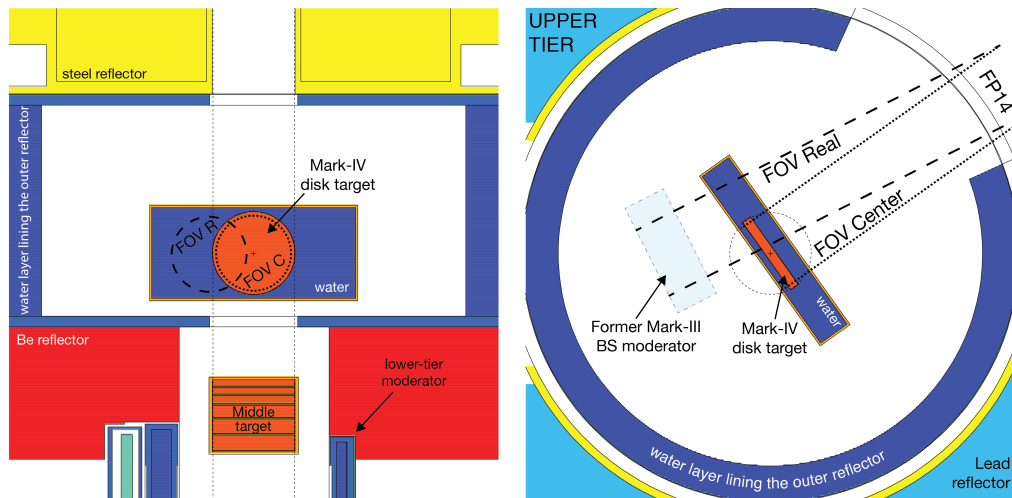


Figure 4: Elevation (left) and plane (right) views of the new Mark-IV upper-tier disk target. FOV Real (FOV R, dashed pattern) represents the 68-cm^2 circular field of view of FP14, formerly focused on the Mark-III backscattering (BS) water moderator, which is no longer present in Mark-IV. FOV Center (FOV C, dotted pattern) is the field of view of the realigned FP14, which focuses on the center of the disk target.

174 3.2.2. Water layer lining the outer lead reflector

175 The removal of the upper-tier beryllium reflector improves the time-emission spectra. Al-
 176 though the overall neutron reflection has been reduced significantly, it has not been eliminated

177 completely due to neutrons being scattered back from the outer lead reflector-shield. To mini-
 178 mize the contribution of these back-scattered neutrons to the tails of the time-emission spectra,
 179 an additional layer of absorbing material needs to be installed in front of the lead reflector.

180 A number of materials with a large neutron absorption cross section in the intermediate-
 181 energy region, such as Eu, Gd, or Ta, were selected for the MCNPX optimization study. However,
 182 none of the candidate materials were able to reduce the tails more efficiently than a layer of water
 183 in a thin aluminum container. The optimal thickness of water was found to be 4 cm. A thinner
 184 layer does not block the reflected neutrons sufficiently, whereas increasing the thickness does not
 185 result in any obvious improvement.

186 The effect of the water layer is shown in Figure 5, where we present the time-emission spec-
 187 tra for 100-eV neutrons as an example of general behavior. The absorption performance of water
 188 is compared with the performance of Eu, Gd, and Ta and it is also compared with a hypothet-
 189 ical case in which no neutron reflection occurs. This neutron trap was achieved by setting the
 190 neutron importance of the layer to zero. Figure 5 also shows that the 4-cm water layer has not
 191 only reduced the tails of the time-emission spectra but has also increased the relative number of
 192 neutrons within 1/10 of the pulse maximum (FWTM), specifically from 79% to 86%.

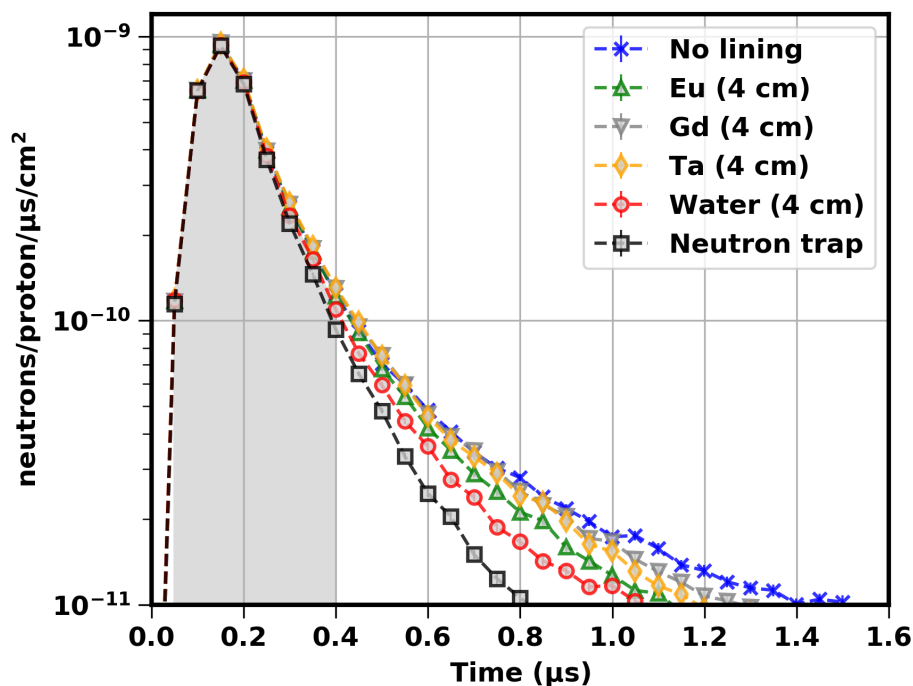


Figure 5: A 4-cm-thick water layer (red circles) lining the outer lead reflector significantly reduces the tails of the time-emission spectra in comparison with no lining present (blue crosses). Zero reflection resulting from a total neutron absorption in the lining is shown by black squares. Absorption performance of 4-cm-thick layers of Eu, Gd, and Ta is shown by green, grey, and yellow symbols, respectively. The grey area represents a region within 1/10 of the pulse maximum (FWTM) of the time-emission spectra for 100-eV neutrons.

193 *3.2.3. Water layer separating upper tier from lower tier*

194 Although the beryllium reflector was removed from the upper tier, its removal from the lower
195 tier is not an option as it would degrade neutron flux for materials research. Neutrons originating
196 in the lower tier can potentially—after a few scattering events in the reflector and thus with a sig-
197 nificant time delay—reach upper-tier FPs, which obviously degrades the time-emission spectra.
198 To avoid such degradation, a maximum neutronic separation of the upper and lower tiers must
199 be achieved.

200 In Mark-III TMRS, a water-cooled aluminum heatsink plate separates both tiers. The alu-
201 minium partition reduces only partially the number of neutrons arriving from the lower tier to
202 the upper tier. To enhance the separation, Monte Carlo calculations were performed for different
203 material compositions and thicknesses of the partition. As with the layer lining the outer lead
204 reflector, it turned out that the water layer is most effective in reducing the asymmetric tails of
205 the time-emission spectra. The optimal thickness was found to be 3 cm.

206 In Figure 6 we compare the upper-tier time-emission spectra of 100 eV neutrons for three
207 different partitions: the current 1.27-cm-thick aluminum heatsink plate, a 3-cm water layer, and
208 an ideal, fully absorbing partition (neutron trap). Although the water partition cannot compete
209 with the neutron trap, it reduces the tails of the time-emission spectra significantly. The partition
210 further increases the relative number of neutrons emitted within FWTM of the time-emission
211 spectra from 86% to 89%. Thus the water layers in front of the lead reflector and between the
212 lower and upper tiers encompass almost 90% of all neutrons within FWTM, which has a positive
213 impact on a large number of experiments.

214 *3.2.4. Mark-IV neutronic performance*

215 The removal of the upper-tier beryllium reflector and backscattering moderators and the in-
216 stallation of the additional disk target and water partitions improve intensity and time resolution
217 for nuclear science. Figure 7 compares the Mark-III neutron flux and time resolution with the
218 anticipated neutronic performance of Mark-IV.

219 As shown in Figure 7, the new target performs better in a wide interval of energies. For
220 example, at 100 keV, the neutron intensity will improve by a factor of 10 if the FOV Center is
221 implemented, whereas only by a factor of 5 if FPs remain in their current configuration (FOV
222 Real). At the same energy, the time resolution for Mark-IV FOV Center shows an improvement
223 by a factor of ~ 12 . The time resolution for FOV Real is about 20% worse in comparison with
224 FOV Center in the entire energy interval. It is important to note that the Mark-IV effective flight-
225 path-length uncertainty is almost independent of the energy in the keV-MeV interval.

226 In Figure 8 we compare figure of merit (FOM, see Equation 1) at FP14 of the new TMRS
227 relatively to Mark-III. At 100 keV, the Mark-IV FOM for FOV Center is better relative to Mark-
228 III by a factor of 1500. FOV Real performs worse by 40% to 70% in comparison with FOV
229 Center, depending on energy. Note that FOM and time resolution consider the TMRS only. Time
230 resolution of the incident proton beam also contributes to the total time resolution, especially at
231 higher energies, as discussed in Section 4.

232 *3.2.5. Gamma-ray background*

233 In addition to neutrons, the spallation process generates a significant amount of charged
234 particles and photons. Whereas the former can be deflected from a FP by a sweeping magnet, an
235 intense flux of the latter—which cannot be suppressed easily—can adversely impact the quality
236 and feasibility of many experiments.

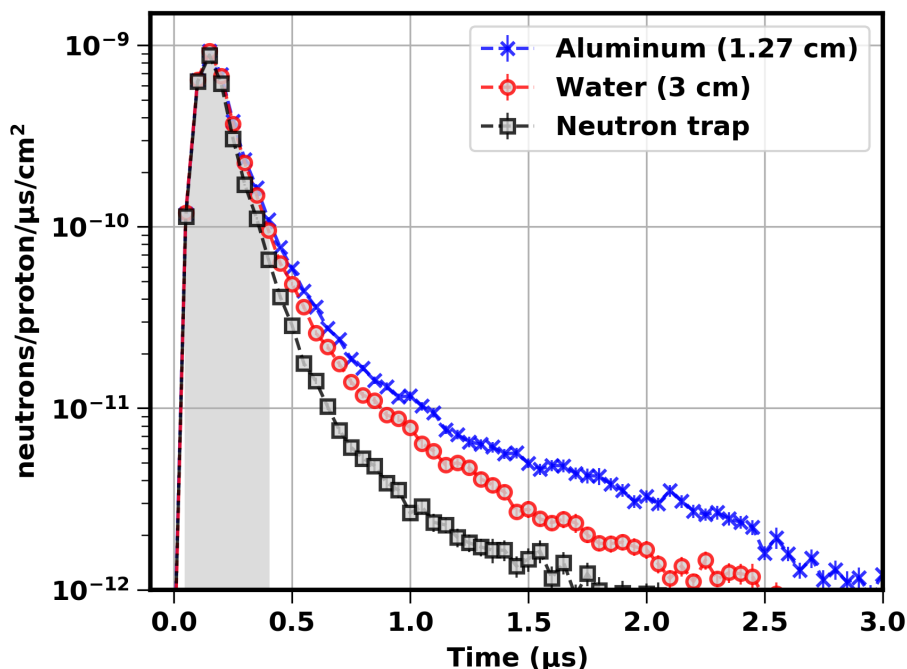


Figure 6: A partition separating upper tier from lower tier is currently made of aluminum (blue crosses). A 3-cm-thick water layer (red circles) will separate the two tiers neutronically in a much more efficient way by reducing the tails of the time-emission spectra. An ideal separation resulting from a total neutron absorption (neutron trap) is represented by black squares.

237 The gamma-ray background from the spallation target typically has two components—prompt
 238 and delayed—and they differ significantly in energy spectra. The prompt component ($\ll 1 \mu\text{s}$)
 239 originates during the spallation process and represents a major part of what is called the γ -flash.
 240 These photons can reach very high energies, depending on parameters of the incident beam.
 241 The delayed component primarily arises from the already-produced neutrons interacting with
 242 the moderator and other materials surrounding the target. The delayed photon flux ($> 1 \mu\text{s}$) has
 243 a softer energy spectrum, with a few isolated peaks characteristic of various physical processes,
 244 such as pair annihilation (511 keV), radiative capture in hydrogen (2.2 MeV), and $^{27}\text{Al}(n,\gamma)$ re-
 245 action (7.7 MeV).

246 Figure 9 shows the MCNPX simulation of the prompt photon flux, and Figure 10 illustrates
 247 the delayed flux in FP14. The results are compared with the photon flux in Mark-III and with
 248 the flux at two relevant neutron time-of-flight experimental facilities: n_TOF [23], [25], and
 249 GELINA [26].

250 The photon flux increases in Mark-IV, where now the upper-tier FPs focus fully (FOV Center)
 251 or partially (FOV Real) on the spallation target, in comparison with Mark-III, where none of the
 252 target is in the FOV of any FPs. Despite increased photon flux, we do not expect any major impact
 253 on the feasibility of most experiments carried out at the Lujan Center, because, in general, the

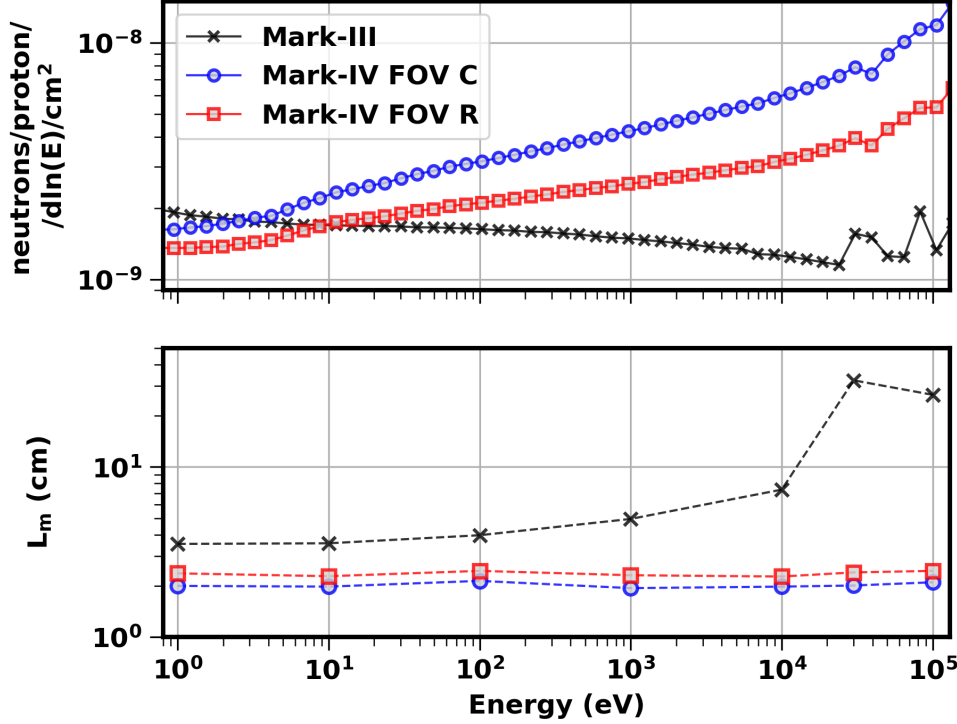


Figure 7: Neutron flux (top) and resolution (bottom) expressed as the effective flight-path-length uncertainty, L_m . We compare the current Mark-III FP14 performance (black crosses) with the Mark-IV data for FOV Center (blue circles) and FOV Real (red squares).

254 photon flux stays below the level of the gamma-ray background at n_TOF, where comparable
 255 experiments are routinely conducted.

256 3.3. Middle target optimization

257 The additional disk target affects the spatial distribution of the neutron generation across the
 258 entire TMRS. An increased production of neutrons in the upper tier leads to an inevitable loss
 259 of neutrons available for the lower tier, where neutrons are produced predominantly from the
 260 spallation process in the middle and lower cylindrical targets. There are no plans to redesign the
 261 lower target, but the MCNPX optimization study of the middle-target thickness was carried out
 262 to maximize the performance of the lower tier. The study examined the integral thermal neutron
 263 flux below 0.5 eV.

264 The original target stack located between the upper and lower tiers of Mark-III (see Figure 1)
 265 was composed of seven tungsten disks with a total thickness of 9 cm. The same set of disks has
 266 already been fabricated as spares. From this stack, a 1.2-cm-thick disk has been utilized for the
 267 Mark-IV upper target (see Section 3.2), and the remaining six disks are available for the middle
 268 target assembly.

269 The results show that the lower-tier thermal neutron flux ranges from 65%, relative to Mark-
 270 III, when no middle target is present, to almost 75% with the full six-disk stack. The latter

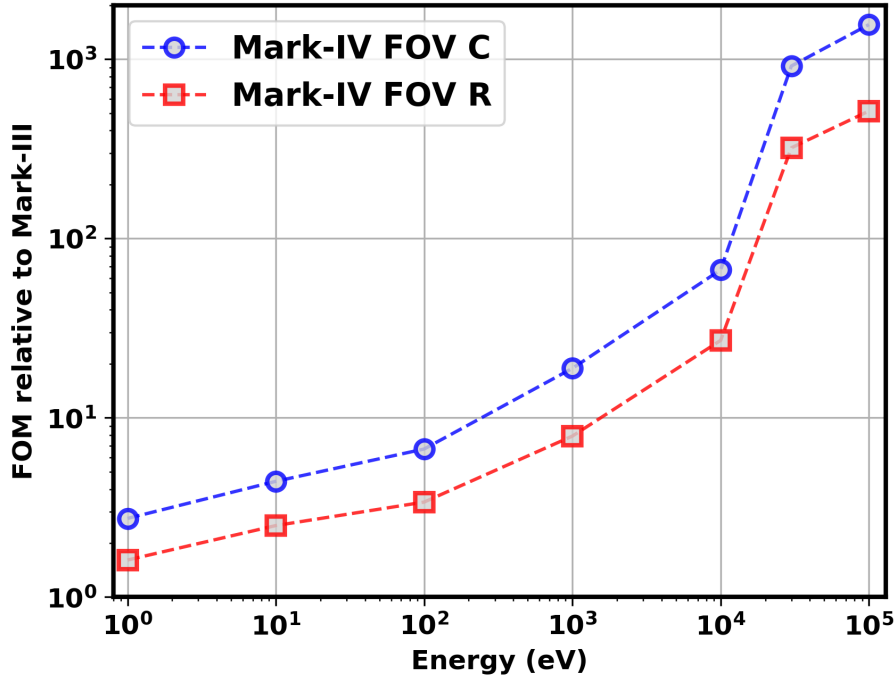


Figure 8: Figure of merit (see Equation 1) of the Mark-IV physics design for FOV Center (blue circles) and FOV Real (red squares) relative to Mark-III.

271 value perfectly matches the key constraint of our study. Therefore, the final configuration of
 272 the middle target comprises six disks with a total thickness of 7.8 cm. Although the thermal
 273 flux has declined, there is no change in either the lower-tier time resolution or background from
 274 neutrons with energies above 0.5 eV or from gamma rays. The thermal flux, however, can return
 275 to its original value, or even increase, by revisiting the design of the lower-tier HR moderator, as
 276 discussed in the following section.

277 3.4. Lower tier

278 The current HR moderator is composed of a 2-cm-thick water premoderator and a 1.5-cm-
 279 thick water moderator, separated by a 100- μ m Gd partition. A flagship instrument served by the
 280 HR moderator is the SMARTS spectrometer. About half of diffraction experiments carried out at
 281 SMARTS do not require high time resolution, which allows us to redesign the HR moderator for
 282 a more flexible regime of operation. In this regime, we can maintain high time resolution for a
 283 class of measurements, and we can provide more neutron intensity for other experiments which
 284 do not require such high resolution.

285 A proposed design of the moderator is shown in Figure 11. The thickness of the premoderator
 286 shrank from 2 cm to 1 cm and the moderator cavity was divided into two volumes, separated by
 287 a 0.25-cm-thick aluminum partition. The first cavity, closer to the premoderator, is 1.6 cm thick

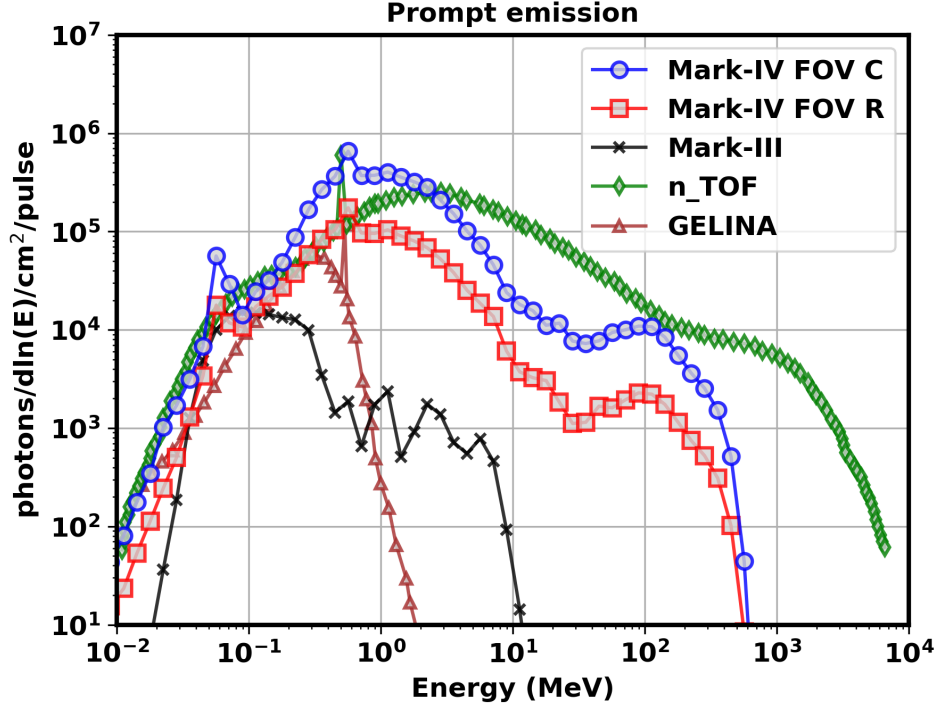


Figure 9: Energy distribution of prompt photon emission at the location of the experiment.

288 and is always filled with water. The other cavity has the same thickness and can be filled with
 289 either water or helium gas. The thickness of the cavity was determined by maximizing FOM for
 290 diffraction experiments at SMARTS according to the equation:

$$FOM_{(SMARTS)} = \int_{0.5\text{\AA}}^{4\text{\AA}} PF(\lambda) d\lambda, \quad (2)$$

291 where $PF(\lambda)$ is peak flux at wavelength λ . When the outboard cavity is filled with water, the
 292 moderator will provide higher neutron flux in the HI mode, whereas when filled with helium gas,
 293 neutrons will be produced in the HR mode, though with lower intensity in comparison with the
 294 HI mode.

295 The HR mode of the newly redesigned moderator does not impact the current time resolution
 296 and provides 6% more thermal neutron flux, because it is positioned closer to the split tungsten
 297 target. On the flip side, the HR mode results in a slightly elevated (approximately 13%) neu-
 298 tron intensity above 0.5 eV, which is considered a background for thermal-neutron scattering
 299 experiments. A suppression of this background can be addressed by utilizing a T0 chopper.

300 The HI mode increases the thermal neutron flux at the expense of time resolution. Our calcu-
 301 lations indicate that the HI mode will provide approximately 60% more neutrons in the thermal
 302 integral. As shown in Figure 12, the increase is energy dependent and results in the highest en-
 303 hancement in thermal flux (a factor of 2) near the point of maximum of the energy distribution.

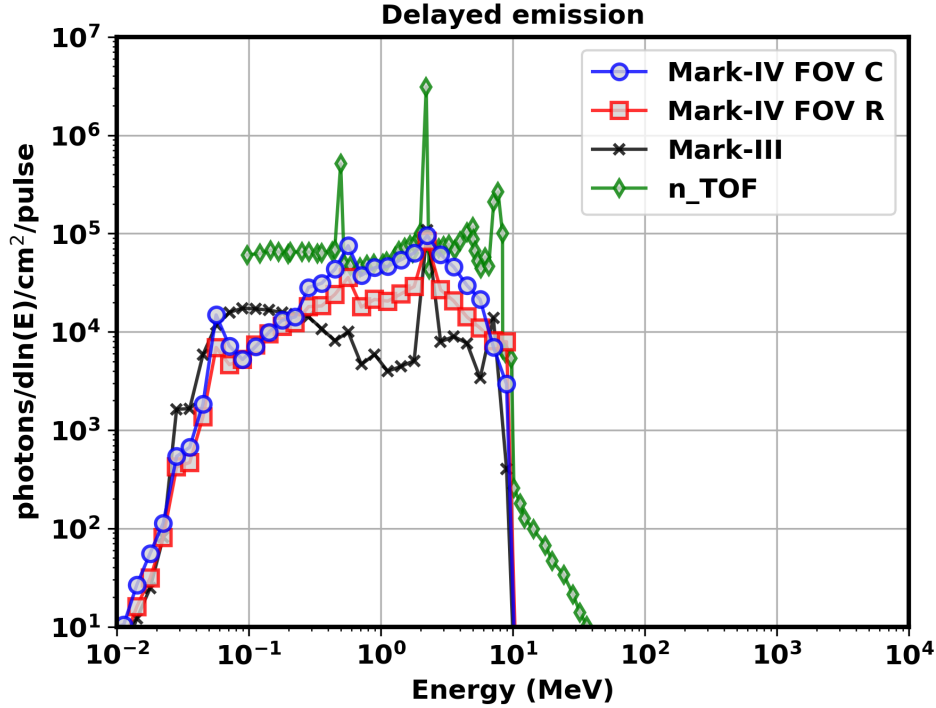


Figure 10: Energy distribution of delayed photon emission at the location of the experiment.

304 In the HI mode, the time resolution of this moderator will resemble the time resolution of the
 305 current HI moderator at FP4. The detailed information about the time resolution of the current
 306 HR and HI moderators can be found in [14].

307 4. Proton beam parameters

308 In Section 3.1 we introduced the resolution (FWHM) of the neutron time-emission spectra
 309 due to moderator, Δt_m . The total resolution of the TMRS Δt_{tot} , however, has another component
 310 reflecting the incident proton beam width Δt_p and is defined according to the formula $\Delta t_{tot} =$
 311 $\sqrt{\Delta t_p^2 + \Delta t_m^2}$. In Figure 13, we show the total resolution Δt_{tot} as a function of neutron energy
 312 in the upper tier of Mark-III and Mark-IV. At energies above 100 eV, the data show that the
 313 reduction of the proton beam width from 50 ns to 30 ns (or an even lower value) has almost
 314 no effect in Mark-III. In Mark-IV, however, the total resolution improves. This is because Δt_m
 315 contributes substantially to Δt_{tot} in Mark-III at all energies, whereas in Mark-IV, its contribution
 316 declines with increasing energy.

317 The high-resolution nuclear physics experiments would benefit from operating the Mark-IV
 318 TMRS with the proton beam with FWHM being reduced from the standard value of 125 ns to
 319 30 ns, which may be a reasonable compromise between good resolution and reasonable intensity.
 320 The minimum pulse width at which it makes sense to run the LANSCE proton storage ring is

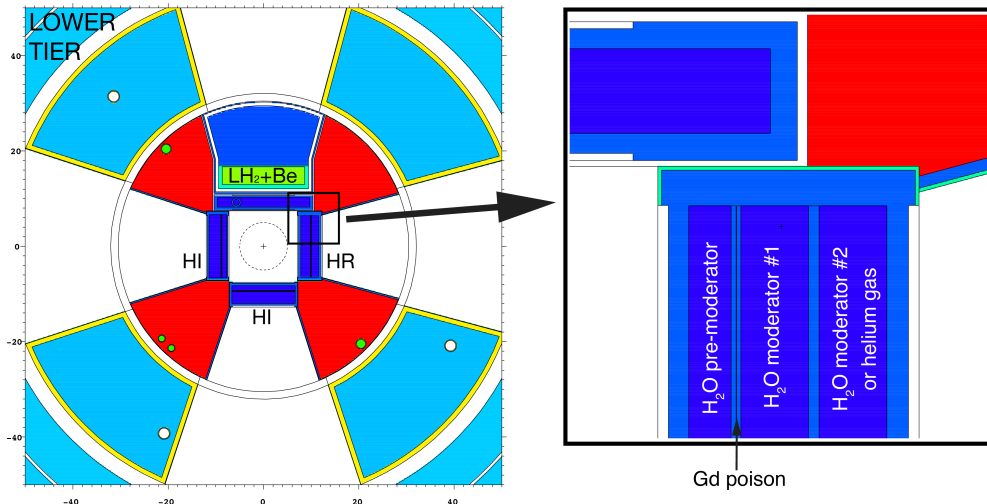


Figure 11: A plane view of the lower tier (left) with a detail of the newly redesigned moderator (right).

321 ~10 ns. With this FWHM, however, the neutron intensity would be reduced by about an order of
 322 magnitude in comparison with the 125-ns pulse.

323 Figure 14 illustrates the expected improvement in measurements of radiative capture cross
 324 section in ^{61}Ni in the resonance region. The simulation of the (n,γ) measurement was carried
 325 out using the *R*-matrix program SAMMY [27]. The program utilizes the MCNPX-calculated
 326 neutron time-emission spectra convoluted with the triangular proton beam pulse with variable
 327 FWHM (30, 50, and 125 ns). The results show that if the new Mark-IV TMRS is driven by
 328 the 30-ns proton pulses, many more resonances can be cleanly resolved as compared with the
 329 standard Mark-III operations. Figure 14 also illustrates that the tails of the Mark-III asymmetric
 330 time-emission pulse profiles cause an apparent shift in the energy of the measured resonances.
 331 Because the asymmetry is reduced in Mark-IV, the importance of this effect will diminish.

332 Both nuclear science and many materials research experiments would also benefit from
 333 higher neutron intensity that can be achieved by increasing the standard repetition rate from
 334 20 Hz to 30 Hz (increasing the proton beam current on target from 100 μA to 150 μA).

335 5. Conclusion

336 The physics design of the next-generation spallation neutron TMRS for LANSCE's Lujan
 337 Center was described in this article. The design makes significant modifications to the upper
 338 tier to enable new nuclear science experiments in the keV-MeV energy range and to improve the
 339 quality of the existing experiments in the same energy range. Minor design modifications were
 340 also implemented to the lower tier to advance its performance in materials research with cold
 341 and thermal neutrons.

342 In the upper tier, removal of the beryllium reflector and backscattering moderators and instal-
 343 lation of the additional spallation target (1.2-cm-thick tungsten disk perpendicular to the existing
 344 target) surrounded by the water moderator will increase the keV-MeV neutron flux and improve
 345 its time resolution. The maximum performance gains will be achieved only if the flight paths

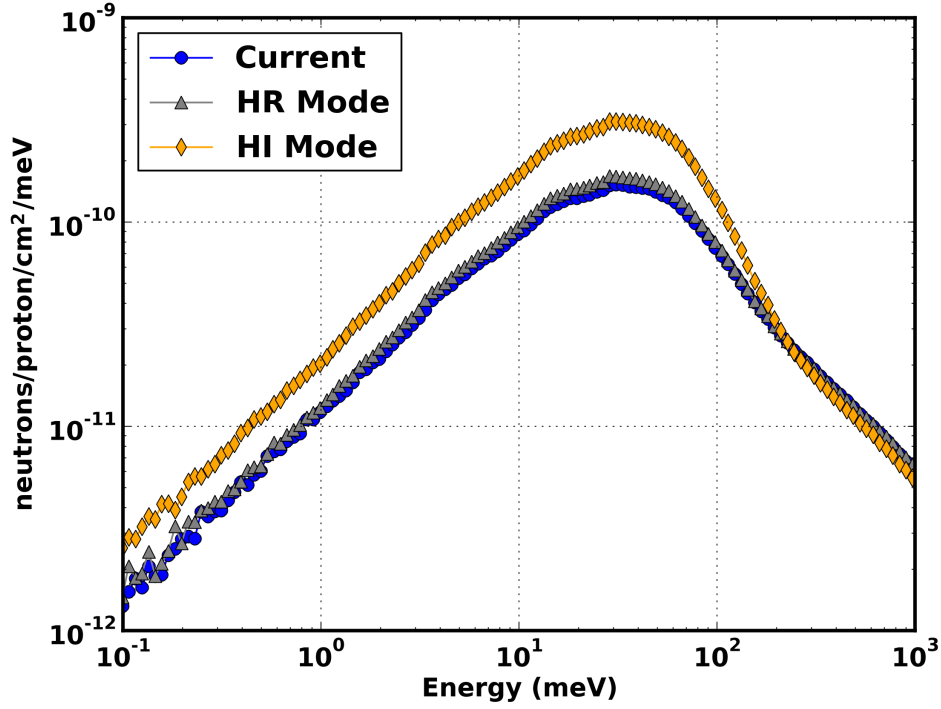


Figure 12: Neutron energy spectra calculated for the high-resolution (HR) mode and high-intensity (HI) mode of the redesigned moderator are compared with the performance of Mark-III at 10 m with $12 \times 12 \text{ cm}^2$ FOV.

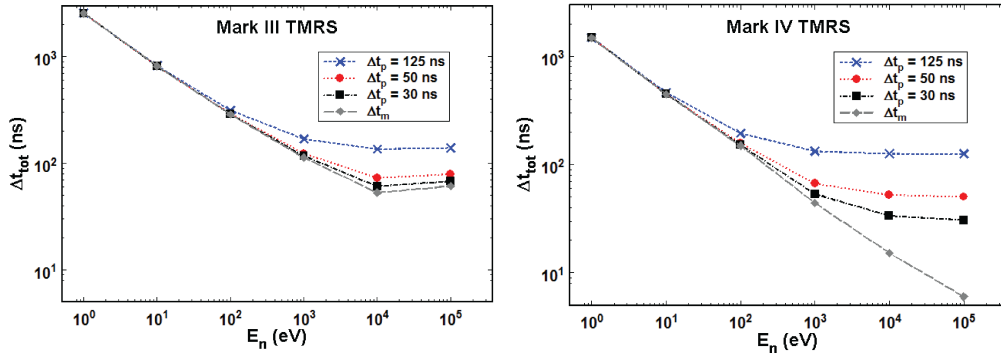


Figure 13: Total time resolution (FWHM), Δt_{tot} , expressed as a contribution from the moderator, Δt_m , together with different proton-beam pulse widths, Δt_p , is shown for the Mark-III and Mark-IV upper-tier FP14 on the left and on the right, respectively.

346 are adjusted to focus directly on the new target. In this configuration, FOM will improve by a
 347 factor of 1500 at 100 keV. On the other hand, the calculations predict a moderate elevation of the
 348 gamma-ray background, which remains below the level of the photon flux at n_TOF.

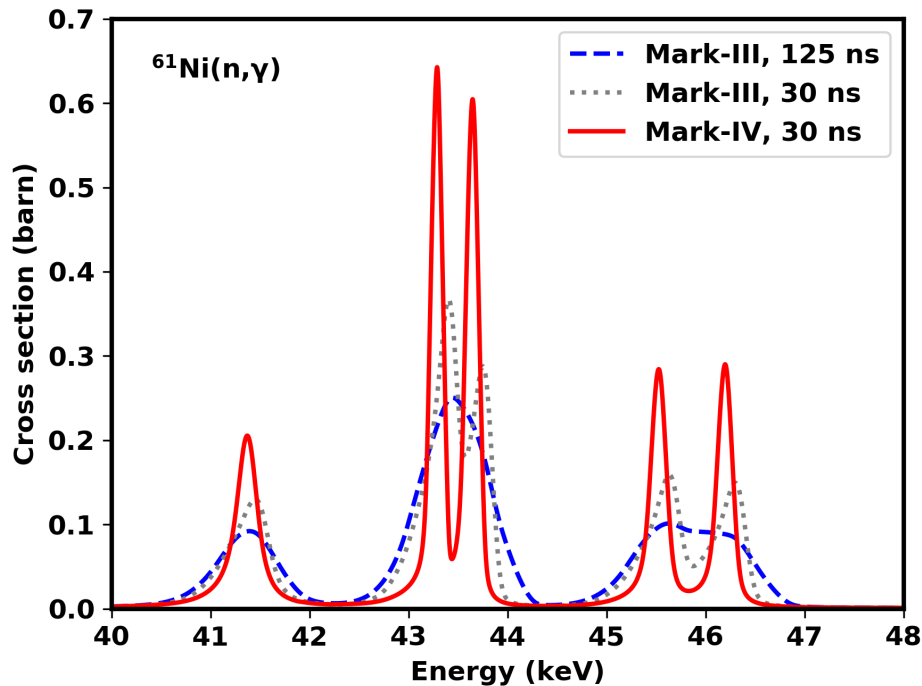


Figure 14: SAMMY predictions for $^{61}\text{Ni}(n,\gamma)$ measurements. Expected results with the Mark-III TMRS and the standard 125-ns proton pulse width are shown by the dashed blue curve. Expected results with the Mark-III and Mark-IV TMRSs and the 30-ns proton pulse are shown as the dotted gray curve and the solid red curve, respectively.

349 To mitigate the impacts of the upper-tier modifications on the lower-tier flux, we have re-
 350 designed the HR water moderator to operate in either HR or HI modes.

351 To access all the advantages offered by the new Lujan TMRS Mark-IV, one needs to tailor
 352 the proton beam characteristics to the experimental needs. Experiments requiring superior time
 353 resolution may sacrifice the proton beam intensity and use narrow proton beam pulses. Other
 354 experiments may need more neutron intensity while tolerating shorter spacing between pulses
 355 accepting 30 Hz repetition rate. And yet different experiments may need standard beam pulse at
 356 20 Hz repetition rate. This flexible regime of operation will inevitably create challenges during
 357 scheduling, but will result in much more effective utilization of the capabilities offered by the
 358 new Lujan TMRS. In this regime, the Lujan Center will serve the needs of the national-security-
 359 related research in a wide interval of neutron energies (cold to intermediate), as well as it will
 360 provide a unique experimental capability for a large number of both national and international
 361 users.

Acknowledgements

The authors would like to acknowledge the entire team supporting the development of the Mark-IV physics design, which includes management, instrument scientists, engineers, techni-

cians, and other staff of the Los Alamos Neutron Science Center.

References

- [1] M. Mocko, G. Muhrer, Fourth-generation spallation neutron target-moderator-reflector-shield assembly at the manuel lujan jr. neutron scattering center, *Nuclear Instruments and Methods in Physics Research Section A: Accelerators, Spectrometers, Detectors and Associated Equipment* 704 (Supplement C) (2013) 27 – 35. doi:<https://doi.org/10.1016/j.nima.2012.11.103>.
URL <http://www.sciencedirect.com/science/article/pii/S0168900212014507>
- [2] P. W. Lisowski, K. F. Schoenberg, The los alamos neutron science center, *Nuclear Instruments and Methods in Physics Research Section A: Accelerators, Spectrometers, Detectors and Associated Equipment* 562 (2) (2006) 910 – 914, proceedings of the 7th International Conference on Accelerator Applications. doi:<https://doi.org/10.1016/j.nima.2006.02.178>.
URL <http://www.sciencedirect.com/science/article/pii/S0168900206003792>
- [3] G. Aliberti, G. Palmiotti, M. Salvatores, T. K. Kim, T. A. Taiwo, M. Anitescu, I. Kodeli, E. Sartori, J. C. Bosq, J. Tommasi, Nuclear data sensitivity, uncertainty, and target accuracy assessment for future nuclear system, *Annals of Nuclear Energy* 33 (2006) 700–733.
- [4] A. Couture, R. Reifarh, Direct measurements of neutron capture on radioactive isotopes, *Atomic Data and Nuclear Data Tables* 93 (5) (2007) 807–830.
- [5] P. Koehler, A. Hayes-Sterbenz, T. Bredeweg, A. Couture, J. Engle, A. Keksis, F. Nortier, J. Ullmann, New opportunity for improved nuclear forensic, radiochemical diagnostics, and nuclear astrophysics: Need for a total-cross-section apparatus at the lansce, la-ur-14-21656.
- [6] P. Koehler, Total cross sections as a surrogate for neutron capture: An opportunity to accurately constrain (n, γ) cross sections for nuclides beyond the reach of direct measurements , la-ur-14-21466.
- [7] S. Mosby, T. Bredeweg, A. Couture, M. Jandel, T. Kawano, J. Ullmann, R. Henderson, C. Wu, $^{239}\text{Pu}(n, \gamma)$ from 10 eV to 1.3 MeV, *Nuclear Data Sheets* 148 (2018) 312 – 321, special Issue on Nuclear Reaction Data. doi:<https://doi.org/10.1016/j.nds.2018.02.007>.
URL <http://www.sciencedirect.com/science/article/pii/S0090375218300267>
- [8] G. Russell, H. Robinson, G. Legate, R. Woods, E. Whitaker, A. Bridge, K. Hughes, The lansce target system, The 9th Meeting of the International Collaboration on Advanced Neutron Sources, Villigen, Switzerland.
- [9] P. Ferguson, G. Russell, E. Pitcher, Proceedings of the International Workshop on Cold Moderators for Pulsed Neutron Sources, Argonne, IL, OECD Brochure (1992) 67 – 72.
- [10] G. Muhrer, P. Ferguson, G. Russell, E. Pitcher, As-built monte carlo model of the lujan target systems and comparison of its neutronic performance to a physics model. Proc. of the Fourth International Topical Meeting on Nuclear Applications of Accelerator Technology (2000) 116.
- [11] T. Ino, M. Ooi, Y. Kiyonagi, Y. Kasugai, F. Maekawa, H. Takada, G. Muhrer, E. J. Pitcher, G. J. Russell, Measurement of neutron beam characteristics at the manuel lujan jr. neutron scattering center, *Nuclear Instruments and Methods in Physics Research Section A: Accelerators, Spectrometers, Detectors and Associated Equipment* 525 (3) (2004) 496 – 510. doi:<https://doi.org/10.1016/j.nima.2004.02.003>.
URL <http://www.sciencedirect.com/science/article/pii/S0168900204002220>
- [12] D. Filges, F. Goldenbaum, *Handbook of spallation research; theory, experiments and application*, wiley-vch (2009) 271.
- [13] M. Dubey, M. S. Jablin, P. Wang, M. Mocko, J. Majewski, Spear — toF neutron reflectometer at the los alamos neutron science center, *The European Physical Journal Plus* 126 (11) (2011) 110. doi:[10.1140/epjp/i2011-11110-1](https://doi.org/10.1140/epjp/i2011-11110-1).
URL <https://doi.org/10.1140/epjp/i2011-11110-1>
- [14] M. Mocko, G. Muhrer, T. Ino, M. Ooi, L. Daemen, Y. Kiyonagi, Monte carlo study of the neutron time emission spectra at the manuel lujan jr. neutron scattering center, *Nuclear Instruments and Methods in Physics Research Section A: Accelerators, Spectrometers, Detectors and Associated Equipment* 594 (3) (2008) 373 – 381. doi:<https://doi.org/10.1016/j.nima.2008.07.034>.
URL <http://www.sciencedirect.com/science/article/pii/S0168900208010115>
- [15] M. Mocko, G. Muhrer, C. Kelsey, M. Duran, F. Tovesson, Experimental measurement of the neutron time-emission spectra at the manuel lujan jr. neutron scattering center, *Nuclear Instruments and Methods in Physics Research Section A: Accelerators, Spectrometers, Detectors and Associated Equipment* 632 (1) (2011) 101 – 108. doi:<https://doi.org/10.1016/j.nima.2010.12.189>.
URL <http://www.sciencedirect.com/science/article/pii/S0168900210029918>
- [16] D. Pelowitz, *Mcnpx user's manual version 2.7.0*, la-cp-11-00438.
- [17] D. Kinsey, *Endf-102 data formats and procedures for the evaluated nuclear data file, endf, endf/b-v*, bnl-ncs-50496.
- [18] V. McLane, et al., *Endf-201 endf/b-vi summary documentation*, bnl-ncs-17541.

- [19] R. MacFarland, New thermal neutron scattering files for endf/b-vi release 2, la-12639-ms.
- [20] J. L. Ullmann, T. Kawano, T. A. Bredeweg, A. Couture, R. C. Haight, M. Jandel, J. M. O'Donnell, R. S. Rundberg, D. J. Vieira, J. B. Wilhelmy, J. A. Becker, A. Chyzh, C. Y. Wu, B. Baramsai, G. E. Mitchell, M. Krtička, Cross section and γ -ray spectra for $^{238}\text{U}(n,\gamma)$ measured with the dance detector array at the los alamos neutron science center, *Phys. Rev. C* 89 (2014) 034603. doi:10.1103/PhysRevC.89.034603. URL <https://link.aps.org/doi/10.1103/PhysRevC.89.034603>
- [21] J. O'Toole, Advances in neutron science instrumentation at the los alamos neutron science center (lansce), in: 2007 IEEE Nuclear Science Symposium Conference Record, Vol. 1, 2007, pp. 627–632. doi:10.1109/NSSMIC.2007.4436411.
- [22] K. Bennett, R. Dreele, H.R. Wenk, Hippo, the high-pressure preferred orientation diffractometer at lansce for characterization of bulk materials, in: ICANS-XV 15th Meeting of the International Collaboration on Advanced Neutron Sources, November 6-9, 2000, Tsukuba, Japan, pp. 473–482.
- [23] C. Guerrero, A. Tsinganis, E. Berthoumieux, M. Barbagallo, F. Belloni, F. Gunsing, C. Weiß, E. Chiaveri, M. Calviani, V. Vlachoudis, S. Altstadt, S. Andriamonje, J. Andrzejewski, L. Audouin, V. Bécaries, F. Bečvář, J. Billowes, V. Boccone, D. Bosnar, M. Brugger, F. Calviño, D. Cano-Ott, C. Carrapiço, F. Cerutti, M. Chin, N. Colonna, G. Cortés, M. A. Cortés-Giraldo, M. Diakaki, C. Domingo-Pardo, I. Duran, R. Dressler, N. Dzysiuk, C. Eleftheriadis, A. Ferrari, K. Fraval, S. Ganesan, A. R. García, G. Giubrone, K. Göbel, M. B. Gómez-Hornillos, I. F. Gonçalves, E. González-Romero, E. Griesmayer, P. Gurusamy, A. Hernández-Prieto, P. Gurusamy, D. G. Jenkins, E. Jericha, Y. Kadi, F. Käppeler, D. Karadimos, N. Kivel, P. Koehler, M. Kokkoris, M. Krtička, J. Kroll, C. Lampoudis, C. Langer, E. Leal-Cidoncha, C. Lederer, H. Leeb, L. S. Leong, R. Losito, A. Manousos, J. Marganiec, T. Martínez, C. Massimi, P. F. Mastinu, M. Mastromarco, M. Meaze, E. Mendoza, A. Mengoni, P. M. Milazzo, F. Mingrone, M. Mirea, W. Mondelaers, T. Papaevangelou, C. Paradela, A. Pavlik, J. Perkowski, A. Plompen, J. Praena, J. M. Quesada, T. Rauscher, R. Reifarth, A. Riego, F. Roman, C. Rubbia, M. Sabate-Gilarte, R. Sarmiento, A. Saxena, P. Schillebeeckx, S. Schmidt, D. Schumann, P. Steinegger, G. Tagliente, J. L. Tain, D. Tarrío, L. Tassan-Got, S. Valenta, G. Vannini, V. Variale, P. Vaz, A. Ventura, R. Versaci, M. J. Vermeulen, R. Vlastou, A. Wallner, T. Ware, M. Weigand, T. Wright, P. Žugec, Performance of the neutron time-of-flight facility n.tof at cern, *The European Physical Journal A* 49 (2) (2013) 27. doi:10.1140/epja/i2013-13027-6. URL <https://doi.org/10.1140/epja/i2013-13027-6>
- [24] C. Coceva, M. Frisoni, M. Magnani, A. Mengoni, On the figure of merit in neutron time-of-flight measurements, *Nuclear Instruments and Methods in Physics Research Section A: Accelerators, Spectrometers, Detectors and Associated Equipment* 489 (1) (2002) 346 – 356. doi:[https://doi.org/10.1016/S0168-9002\(02\)00903-8](https://doi.org/10.1016/S0168-9002(02)00903-8). URL <http://www.sciencedirect.com/science/article/pii/S0168900202009038>
- [25] E. Chiaveri, Proposal for n.tof experimental area 2, cern-intc-2012-029.
- [26] D. Ene, C. Borcea, S. Kopecky, W. Mondelaers, A. Negret, A. Plompen, Global characterisation of the gelina facility for high-resolution neutron time-of-flight measurements by monte carlo simulations, *Nuclear Instruments and Methods in Physics Research Section A: Accelerators, Spectrometers, Detectors and Associated Equipment* 618 (1) (2010) 54 – 68. doi:<https://doi.org/10.1016/j.nima.2010.03.005>. URL <http://www.sciencedirect.com/science/article/pii/S0168900210005589>
- [27] N. Larson, Updated user's guide for sammy: Multilevel r-matrix fits to neutron data using bayes' equations, ornl/tm-9179/r8, endf-364/r2.